DEACTIVATION AND EXCITATION OF OI($6s\ ^5S$) AT

ABOVE-THERMAL ENERGIES

RECOMMENDED:

Gerald J. Romick

Chairman, Advisory Committee

Chairman, Department of Physics

Dean, College of Environmental Sciences

Mary Elizabeth Shuttler
Dean, College of Arts and Sciences

APPROVED: K. B. Clarke
Vice Chancellor for Research and Advanced Study

April 19, 1982
Date

DEACTIVATION AND EXCITATION OF OI($6s\ ^5S$) AT ABOVE-THERMAL ENERGIES

A

THESIS

Presented to the Faculty of the University of Alaska

in Partial Fulfillment of the Requirements

for the Degree of

MASTER OF SCIENCE

By

Joseph Albert Enzweiler, B.S.

Fairbanks, Alaska

May 1982

ABSTRACT

Absolute collisional deactivation and excitation cross sections have been measured for a beam of O (^5P-$^5S^o$) incident on N_2. The beam energy was varied from 3.95 to 10.65 keV. Cross sections for charge transfer (electron capture) of O^+ in N_2 were also measured in the energy range from 2.4 to 24.3 keV.

The variation of light intensity at 5436 Å (from the 6s-3p transition of the quintet system of atomic oxygen) emitted from the beam as a function of N_2 target pressure was fitted to a beam kinetic equation to determine deactivation and excitation cross sections. The cross section for deactivation in N_2 decreases from 6.84×10^{-15} cm^2 at 3.95 keV to 1.5×10^{-15} cm^2 at 19.65 keV. The cross section for excitation decreases from 3.3×10^{-19} at 3.95 keV to 2.25×10^{-19} cm^2 at 19.65 keV.

ACKNOWLEDGEMENTS

At this time I wish to thank the members of my committee, Prof. Charles Deehr, Prof. Stephen Mac Lean, Prof. John Morack, Prof. Gerald Romick, Prof. Roger Sheridan and Prof. Abas Sivjee, for their time in reading this thesis and their helpful comments about the material. I especially thank Prof. Roger Sheridan for his encouragement and help in solving difficult experimental problems, and for needed guidance into a most subtle field of Physics. I owe special thanks to Prof. Abas Sivjee for his encouragement and concern for my future, to Mr. Tom Merlo and Mr. John Wagner for many helpful conversations and for their friendship through it all and to Ms. Nancy Walters for assistance in the typing of the thesis. The work reported here was supported in part by a grant from the National Science Foundation, ATM 74-14428 A01.

TABLE OF CONTENTS

LIST OF FIGURES

1. INTRODUCTION

There is considerable interest in obtaining quantitative measurements for atomic and molecular processes which are important in atmospheric and auroral modeling. A knowledge of reaction rates near room temperature is often insufficient for an accurate and realistic explanation of these processes. Temperatures well above 1000° K occur frequently in the atmosphere above 200 km (CRA, 1965 Model Atmosphere) and under very active conditions, temperatures of 1000° K can occur as low as 160 km. It has been indicated that the range of velocities found in the earth's atmosphere may depart widely from the Maxwell-Boltzmann distribution (Bauer et al., 1971). Furthermore, the need for a study of atomic processes above thermal energies is further supported by recent evidence that heavy ions in the upper ionosphere have energies in the keV range (Shelley et al., 1976; Sharp et al., 1977). It has been suggested that these heavy ions may be selectively heated O^+ ions. Since excited states of neutral oxygen can be formed in a charge transfer reaction involving O^+, reaction rates of both neutral and ionized atomic species are essential before a complete and self-consistent model can be proposed. A comparison of cross section with reaction rate data can be made only if the velocity dependence of the cross sections is known. Thus, a determination of the cross sections for reactions involving excited states of O and O^+ at above-thermal energies, as well as the velocity dependence of these reactions, is most important in the understanding of atmospheric and auroral processes where such excited states are involved.

There has been an interest shown recently in photometric measurements of auroral OI(6300 Å), OI(7774 Å), and OI(8446 Å) emissions (Christensen et al., 1978). Of particular interest has been a detailed examination of the variations in the observed brightness of these emissions. The decrease observed in the ratio I(8446)/I(7774) as I(6300)/I(4278) becomes smaller is contrary to the constant value for I(8446/I(7774) that is expected from electron impact excitation of the OI(7774 Å) and OI(8446 Å) multiplets. The results of this study indicate that an additional excitation mechanism for OI(7774 Å) at relatively low altitudes in aurora is required to explain the OI(7774 Å) intensity.

There are a number of excited states of neutral oxygen which can directly contribute to the population of the $3p\ ^5P$ energy level (which produces the 7774 Å emission). Among these is the $6s\ ^5S$ state, which decays into the $3p\ ^5S$ level by spontaneous radiative decay. The lifetime of the $6s\ ^5S$ state is reported as .328 μsec. (Weise et al., 1966). Deactivation and excitation cross sections for this state have not been measured at any energy. In light of the present failure in determining a reasonable mechanism to explain the OI(7774 Å) intensity, a knowledge of the above cross sections for an excited state that will contribute to the OI(7774 Å) emission may be of use in obtaining a more complete picture of this particular auroral process.

A new technique has been developed to measure the absolute deactivation cross section for the $OI(6s\ ^5S)$ state on N_2 at energies between 3.95 and 19.65 keV. The technique involves passing a beam of neutral

atomic oxygen through a collision chamber and measuring the variation in intensity of the 5436 Å (6s-3p) optical emission as a function of target pressure. The observed variation is then fitted to a "beam dynamic" equation. This fit yields values of two parameters, one of which is the deactivation cross section, σ_d; the other parameter, B, is proportional to the excitation cross section, σ^*. An extention of the technique involves the determination of absolute values of σ^* by an absolute calibration of the overall detection efficiency of the system, using the known cross section for production of H_α (6563 Å) by collisions of protons with N_2 as a standard. σ^* can be determined for the same energy range as σ_d. In addition, charge transfer measurements and stripping (σ_{01}) cross sections were carried out.

The technique used for measurement of deactivation cross sections in the present experiment is best suited for measurements of these cross sections involving states with natural lifetimes of .1 to 1 μsec.

Although no previous measurements of excitation or collisional deactivation of the 6s ^5S state of oxygen have been carried out, there are certain general features of excitation and collisional deactivation which can be mentioned. The variation of optical signal with target pressure should in general show a linear increase at lower pressures, where excitation is proportional to target density. At higher pressures, however, the signal will not rise in the same way with pressure, since various other channels for excitation and deactivation become significant in quenching the excited state. Below is a list of some processes which cause changes in the internal energy structure of a

particle and as a result act as a deactivation mechanism for the excited state of interest:

a) radiative transition to any lower state

b) electron capture or electron loss

c) excitation to higher states

d) excitation transfer to the target (N_2 in the present experiment)

We could also expect the collisional deactivation cross section to be large in the same region where the excitation cross section is large. An interaction between particles which becomes stronger as a certain energy is reached should enhance the effects of both excitation and quenching. The adiabatic criterion, when applied to the 6s excited state of O, predicts that the cross section for deactivation and excitation should peak at high energy. However, if curve crossing of the colliding species takes place, the effective energy defect, ΔE, becomes small. This will result in a shift of the predicted cross section maxima to lower energies (assuming we apply the adiabatic criterion equally to the endothermic process of excitation and the exothermic process of deactivation).

2. BEAM DYNAMICS

The method used in the present study to observe the interaction between the beam and target gas is to detect photons emitted for a particular optical transition resulting from collisions. The wavelength of the emission characterizes the state under observation. This allows a direct means of determining the cross section for deactivation and excitation of the state of interest. In this case, a beam of neutral atomic oxygen is partially excited in collisions with N_2 target gas, producing the 5436 Å ($6s^5S^o-3p^5P$) optical emission of interest. This section develops the expression for the number density of excited atomic oxygen atoms in the beam and the corresponding equation for optical signal. The data for the observed optical signal divided by the measured beam current was fitted to the final expression for signal/I_s (where I_s is the measured current). This fit yielded the values of the deactivation and excitation cross sections for the O^*-N_2 reaction.

A beam of particles colliding with a target gas will be attenuated by collisional scattering. This interaction of beam and target can cause a change in the internal energy of one or both colliding particles. Below is a list of the kinds of collisions that have possible importance in the present study:

a) charge transfer: $O^+ + N_2 \longrightarrow O + N_2^+$

b) stripping: $O + N_2 \longrightarrow O^+ + N_2 + e$

c) excitation: $O + N_2 \longrightarrow O^* + N_2$

d) collisional deactivation: $O^* + N_2 \longrightarrow O + N_2$

e) radiative decay: $O^* \longrightarrow O + h\nu$

Production of new excited particles in the beam is due to collisions with the target gas. The number of excited particles per unit time produced at any point will, therefore, increase linearly with target density. A particle in the excited state will decay to a lower energy level in a time characteristic of the particular state and independent of target density (the radiative lifetime). If collisional deactivation were <u>not</u> present, the intensity of photon emission would show a linear increase with target density. If, however, further collisions of the excited beam particles with the target occur, causing deactivation prior to radiative decay, the result will be a deviation from this linear trend. Thus the manner in which the intensity of photon emission varies with target density provides the necessary information to determine the deactivation and excitation cross sections.

The process of charge transfer, whereby an O^+ ion acquires an electron from a target molecule, forming neutral atomic oxygen ($O^+ + N_2 \longrightarrow O + N_2^+$), increases the number of neutrals in the beam. Stripping of an electron from neutral oxygen atoms in collisions ($O + N_2 \longrightarrow O^+ + N_2 + e$) decreases the number of neutrals. Thus the net rate of production of ions and neutrals is given by the set of equations

$$\frac{\partial n^+}{\partial t} = v\sigma_{01} n^o n_t - v\sigma_{10} n^+ n_t \qquad (2.1)$$

and $$\frac{\partial n^o}{\partial t} = v\sigma_{10} n^+ n_t - v\sigma_{01} n^o n_t \qquad (2.2)$$

where n^o and n^+ are the number densities for neutral and ionized oxygen atoms, respectively; σ_{01} and σ_{10} are the cross sections for stripping and charge transfer. Assuming steady state conditions, n^+ and n^o at any given position will not change in time. Thus the rate of production of each of these species within a volume equals the net flux of each out of the volume. We may then write

$$\frac{dn^+}{dx} = \sigma_{01} n^o n_t - \sigma_{10} n^+ n_t \qquad (2.3)$$

$$\frac{dn^o}{dx} = \sigma_{10} n^+ n_t - \sigma_{01} n^o n_t \qquad (2.4)$$

We assume solutions of the form

$$n^+ = A + Be^{-\beta x} \qquad (2.5)$$

$$n^o = C + De^{-\beta x} \qquad (2.6)$$

By substituting these into (2.3) and (2.4), we can evaluate C and D in terms of A and B and solve for β. Thus we have

$$n^+ = A + Be^{-\beta x} \qquad (2.7$$

and $$n^o = \frac{\sigma_{10}}{\sigma_{01}} A - Be^{-\beta x} \tag{2.8}$$

where $\beta = (\sigma_{01} + \sigma_{10})n_t$. For our optical measurements, the beam is all neutral at $x = 0$, since all ions are removed from the beam at that point. Thus $n^+ = 0$ and $x = 0$. Applying this initial condition to (2.7) and (2.8) gives

$$n^+ = fn_o (1 - e^{-\beta x}) \tag{2.9}$$

$$n^o = gn_o (1 - e^{-\beta x}) + n_o e^{-\beta x} \tag{2.10}$$

where n_o denotes the number density of neutrals at $x = 0$, and

$$f = \frac{\sigma_{01}}{\sigma_{01} + \sigma_{10}} \quad \text{and} \quad g = \frac{\sigma_{10}}{\sigma_{01} + \sigma_{10}}$$

Experimentally we have observed that the stripping cross section (reaction b) is extremely small. The ratio of the stripping to the charge transfer cross section was measured to be .013 at 10 keV.

We may say then, since $g >> f$ ($\sigma_{10} >> \sigma_{01}$), that n^o is constant, i.e., $n^o = n_o$. This can be seen in (2.10), which can be written as

$$gn_o + fn_o e^{-\beta x}$$

For $g >> f$, the position dependent term is negligible.

The rate of change of the number density, n*, of an excited atomic state in the beam resulting from direct collisional excitation is given by $v\sigma n^{o} n_t$. n_t is the target number density and is related to the pressure by $n_t = 3.152 \times 10^{12}$ p, where p is the pressure in units of 10^{-4} torr. σ^* is the cross section for excitation of an incident neutral oxygen atom to the state of interest (in this case $6s\ ^5S^o$) in a collision with a target molecule.

The rate of loss of n* by spontaneous radiative decay is given by n^*/τ, where τ is the radiative lifetime of the state of interest. The rate of loss of n* by collisional deactivation is given by $n^* n_t \sigma_d v$, where σ_d is the cross section for deactivation of an atom from the excited state of interest as a result of a collision with a target particle. Thus the net rate of change of the number density of particles in the excited state is

$$\frac{\partial n^*}{\partial t} = v\sigma^* n^{o} n_t - v\sigma_d n^* n_t - n^*/\tau \qquad (2.11)$$

In the steady state case, n* at any given position does not change in time. We can then say that the rate of production of n* within a volume equals the net flux of excited particles out of the volume. Thus

$$v \frac{\partial n^*}{\partial x} = v\sigma^* n^{o} n_t - v\sigma_d n^* n_t - n^*/\tau \qquad (2.12)$$

This is the continuity equation for the number of particles in the excited state at any point along the beam axis (x-axis). Spreading of the beam along the axis has been neglected, since the viewing region is not limited top to bottom. Also, the Faraday cup which receives the current is sufficiently large to accommodate any beam spreading that may occur. We may rewrite (2.12) as

$$\frac{\partial n^*}{\partial x} = \sigma^* n^o n_t - \sigma_d n^* n_t - n^* / v\tau \qquad (2.13)$$

We have seen that n^o can be considered constant and can be replaced by n_o, the initial density of neutral atoms in the beam. The solution of this equation has the form $n^* = A + Be^{-\beta x}$. Substituting this form into (2.13) and equating coefficients of like terms yields the expression

$$n^* = \frac{\sigma^* n_o n_t}{\alpha} (1 - e^{-\alpha x}) + n_o^* e^{-\alpha x} \qquad (2.14)$$

where n_0^* is n^* at $x = 0$ and $\alpha = \sigma_d n_t + 1/v\tau$. Dividing by n_o, we have

$$\frac{n^*}{n_o} = \frac{\sigma^* n_t}{\alpha} (1 - e^{-\alpha x}) + f^* e^{-\alpha x} \qquad (2.15)$$

Here $f^* = n_o^*/n_o$ represents the fraction of excited particles in the beam at $x = 0$.

Omitted from the equation is the effect of cascade, whereby particles are excited to higher energy levels and decay into the level of interest. Cascade would increase the number density, n*, of particles in the state of interest and the effective excitation cross section σ* as well. A term $n_k^* A_{ki}$ would be added to the right hand side of (2.12) where n_k^* is the number density of particles in the k th state and A_{ki} the corresponding transition probability from the k th state into the state of interest. n_k^* has a form similar to n*, i.e.,

$$n_k^* = \frac{\sigma_k^* n_t n_o}{\alpha'} (1 - e^{-\alpha' x}) + f^{*\prime} n_o e^{-\alpha' x}$$

σ_k^* is the cross section for exciting a particle into the k th energy level. $\alpha' = \sigma_d' n_t + 1/v\tau'$ and $f^{*\prime} = n_o^{*\prime}/n_o$. Primed symbols represent quantities corresponding to a higher energy level than the one of interest. If we consider the lifetimes of these upper states to be short (τ' is small), $\sigma_d' n_t$ will be much smaller than $1/v\tau'$; the exponential terms will also be small. Retaining only the dominant terms in the expression, we have

$$n_k^* = \sigma_k^* n_t n_o v\tau'$$

Therefore we will have one additional term in (2.12). The expression becomes

$$v\frac{dn^*}{dx} = v\sigma^* n_o n_t - n^*/\tau - v\sigma_d n^* n_t + v\sigma_k^* n_o n_t A_{ki}\tau'$$

Letting $f_{ki} = A_{ki}\tau'$, the fraction decaying from the k th into the i th state, we see that σ^* will effectively be increased to the new value $\sigma^* + \Sigma\sigma_k^* f_{ki}$. Here we have summed over all higher states. The cross sections σ_k^* for excitation into levels higher than the 6s are not known, but it is assumed that these numbers are relatively small. Furthermore, the quantities f_{ki} are all very small, since most quintet p states decay via transitions to the $3\,^5S$ state. Thus the correction to σ^* from cascade effects should be quite small.

The number of photons J emitted per unit time from a small segment of the beam having path length L and cross sectional area A can be expressed as $J = n^* ALA_{ij}$, where A_{ij} is the transition probability per unit time for radiative decay from energy level i to j. The signal that is detected by a photometer will be directly proportional to J, the constant of proportionality being the overall detection efficiency η_{6s}, so that signal = $\eta_{6s} J$. The current measured in the experiment is the current from secondary electrons produced at the detector from impact of neutrals. This current is related to n^o by the equation $I_s = n^o evA\eta$, where η is the secondary emission coefficient. Since we have set $n^o = n_o$, the signal divided by the measured secondary emission current is given by

$$\frac{\text{signal}}{I_s} = \frac{n^* LA_{ij}\eta_{6s}}{n_o ev\eta} \qquad (2.16)$$

Substituting n^*/n_o from (2.15) gives

$$\frac{\text{signal}}{I_s} = \frac{\eta_6 s A_{ij} L}{ev\eta}\left[\frac{\sigma^* n_t}{\alpha}(1 - e^{-\alpha x}) + f^* e^{-\alpha x}\right] \qquad (2.17)$$

Experimentally we can use this equation in one of two ways. The right hand side can be considered either as a function of x with fixed pressure or, as in the present experiment, a function of pressure with fixed x.

In the present experiment the beam passes through three different collision regions. Equation (2.15) can be applied separately to each region, with the f* for one region being the final value of n^*/n_o for the region just preceding it. When this is done, the expression for n^*/n_o at the position of the detector is

$$\frac{n^*}{n_o} = \frac{\sigma^* n_3}{\alpha_3}(1 - e^{-\alpha_3 x_3}) + e^{-\alpha_3 x_3}\left[\frac{\sigma^* n_2}{\alpha_2}(1 - e^{-\alpha_2 x_2}) + e^{-\alpha_2 x_2}\left\{\frac{\sigma^* n_1}{\alpha_1}(1 - e^{-\alpha_1 x_1}) + f^* e^{-\alpha_1 x_1}\right\}\right] \qquad (2.18)$$

where subscripts 1, 2 and 3 respectively refer to the first, second and third collision region encountered by the atomic beam. When (2.18) is substituted for n^*/n_o in (2.16), one obtains

$$\frac{\text{signal}}{I_s} = \frac{\eta_{6s} A_{ij} L}{ev\eta} \left[\frac{\sigma^* n_3}{\alpha_3} (1 - e^{-\alpha_3 x_3}) + e^{-\alpha_3 x_3} \left\{ \frac{\sigma^* n_2}{\alpha_2} (1 - e^{-\alpha_2 x_2}) + e^{-\alpha_2 x_2} \left[\frac{\sigma^* n_1}{\alpha_1} (1 - e^{-\alpha_1 x_1}) + f^* e^{-\alpha_1 x_1} \right] \right\} \right] \tag{2.19}$$

This can be rewritten as

$$\frac{\text{signal}}{I_s} = Ae^{-\Sigma\alpha_i x_i} + B \left[\frac{\eta_1}{\alpha_1} (e^{-(\alpha_2 x_2 + \alpha_3 x_3)} - e^{-\Sigma\alpha_i x_i}) + \frac{\eta_2}{\alpha_2} (e^{-\alpha_3 x_3} - e^{-(\alpha_2 x_2 + \alpha_3 x_3)}) + \frac{\eta_3}{\alpha_3} (1 - e^{-\alpha_3 x_3}) \right] \tag{2.20}$$

where $A = Df^*$, $B = D\sigma^*$ and $D = (\eta_{6s} A_{ij} L)/ev\eta$. The three unknown parameters are A, B and σ_d. σ_d is included in the α_i terms. For the conditions of this experiment, the term $Ae^{-\Sigma\alpha_i x_i}$ can be neglected, since the ratio of this term to the dominant term (Bn_3/α_3) is

$$\frac{f^* e^{-\Sigma\alpha_i x_i} \alpha_3}{n_3 \sigma^*}$$

Since $1/v\tau$ is always greater than $n_i\sigma_d$, α_i can be approximated by $1/v\tau$, and this ratio is approximately

$$\frac{f^* e^{-\Sigma x_i/v\tau}}{n_3 \sigma^* v\tau}$$

using the largest probable value for f* (.01) and the smallest probable value for $\sigma^*(10^{-18}\ cm^2)$, and using typical values for n_3 and v, the ratio has the value .0018. The term $Ae^{-\Sigma\alpha_i x_i}$ is thus clearly negligible.

One can record the signal, S, and the measured current, I_s, at a number of different target pressures. Equation (2.20) can then be fitted to the experimental values for signal/I_s. This involves adjusting the values of both parameters B and σ_d to give the best fit.

Having developed the theoretical expressions used in the present study, we next describe the apparatus and experimental procedure.

3. EXPERIMENTAL DETAILS

Apparatus

The basic apparatus is described elsewhere (Suchannek, 1974; Vidmar, 1974), so only modifications of the apparatus will be described in detail here.

O^+ ions produced in a radio-frequency discharge in oxygen are accelerated and mass analyzed before entering a charge exchange cell. Here a fraction of O^+ ions undergo charge exchange in collisions with N_2. The beam then passes through an electrostatic field which separates the ions from the neutrals. The neutral beam enters the collision chamber and interacts with the target gas. After the beam passes through the target chamber and into a lower pressure observation chamber, light emitted from a small segment of the beam is detected by a photometer. The flux of the neutral beam can be measured by measuring the secondary emission it produces upon striking a metal surface. Particle energies ranged from 3.95 to 19.65 keV and secondary emission current ranged from 5×10^{-9} to 3×10^{-7} amps.

A schematic of the three chambers is shown in Figure 3.1. Small apertures at both ends of the target chamber allow passage of the beam, while essentially confining the target gas within the chamber via differential pumping. The apertures are adjustable to allow for proper beam alignment. The inside of the chamber as well as the aperture openings are coated with colloidal graphite to eliminate reflection of light from these surfaces into the photometer and to reduce charge

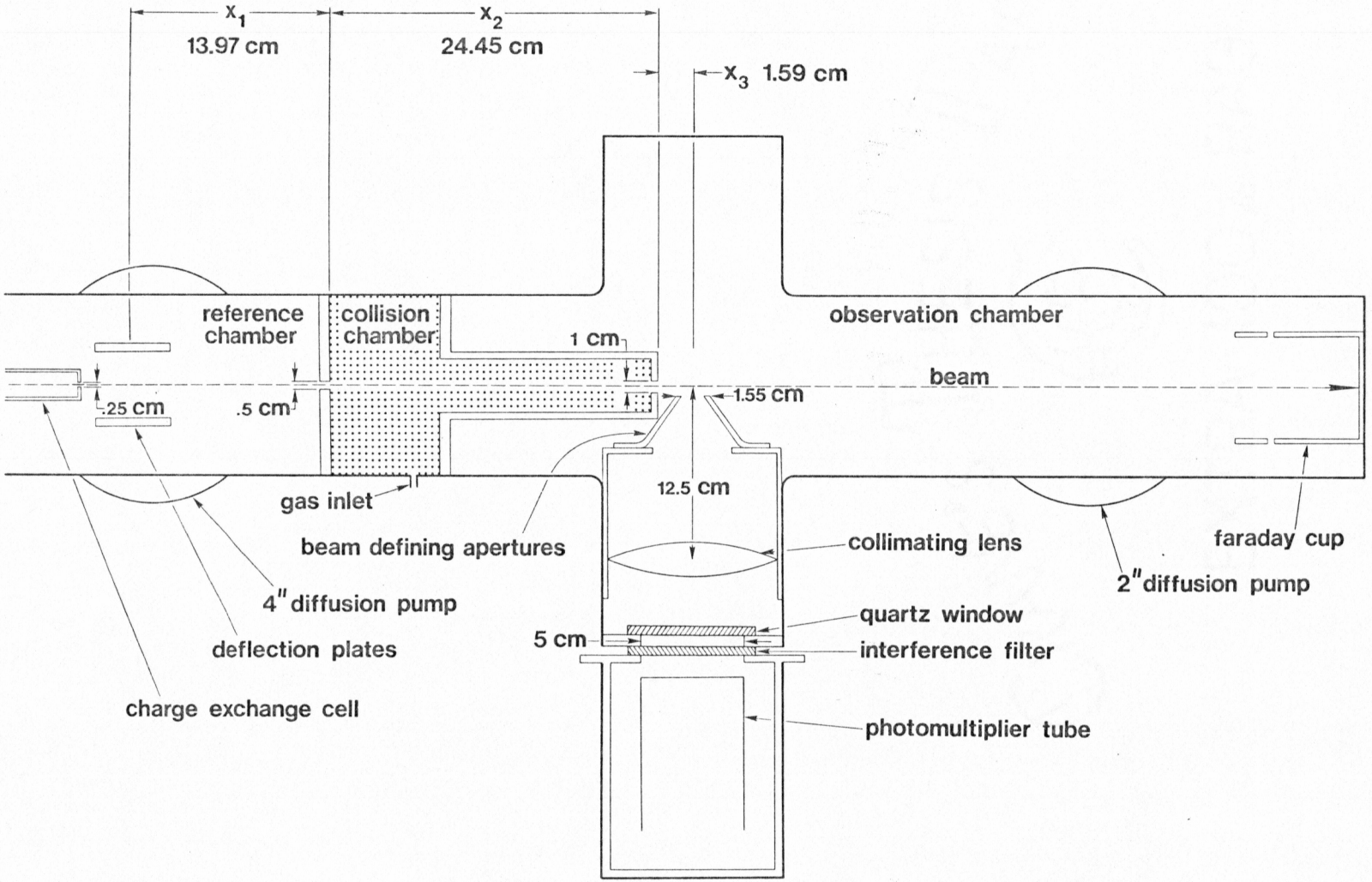

Fig. 3.1. Schematic of experimental apparatus

build-up on the surfaces. The target chamber is equipped with a leak valve to admit the target gas. A capacitance manometer measures the differential pressure between the target chamber and the lower pressure region of chamber 1 ("reference chamber"). The absolute pressure in chambers 1 and 3 is measured using ionization gauges. Chambers 1 and 3 are provided with 4 inch and 2 inch diffusion pumps, respectively. A photometer, consisting of a photomultiplier tube and an interference filter, is mounted to the observation chamber, directly in front of a quartz window. The optical axis of the photometer is perpendicular to the beam axis. A pair of light baffles mounted to a plate with a 3 cm. hole is placed between the beam and the photometer to limit vignetting. The beam diameter is less than 3 cm.; thus, none of the beam is obscured, top to bottom. A collimating lens is placed at a distance equal to its focal length from the beam to collimate the light entering the photometer. The interference filter used had a peak transmission at 5436 Å with a bandpass of 12.5 Å (see Figure 3.2).

A Faraday cup is mounted at the end of the observation chamber to measure the beam flux. When neutral atoms strike the metal surface of the cup, secondary electrons are produced. A positive potential of 100 volts applied to the guard ring is sufficient to insure that all secondary electrons produced by the beam will be removed from the cup and a net positive current will be observed at the Faraday cup. When a beam of positive ions strikes the cup, 100 volts negative is applied to the guard ring, thus suppressing secondary electrons and leaving only the ion current. When the beam is a composite of neutrals and ions, the

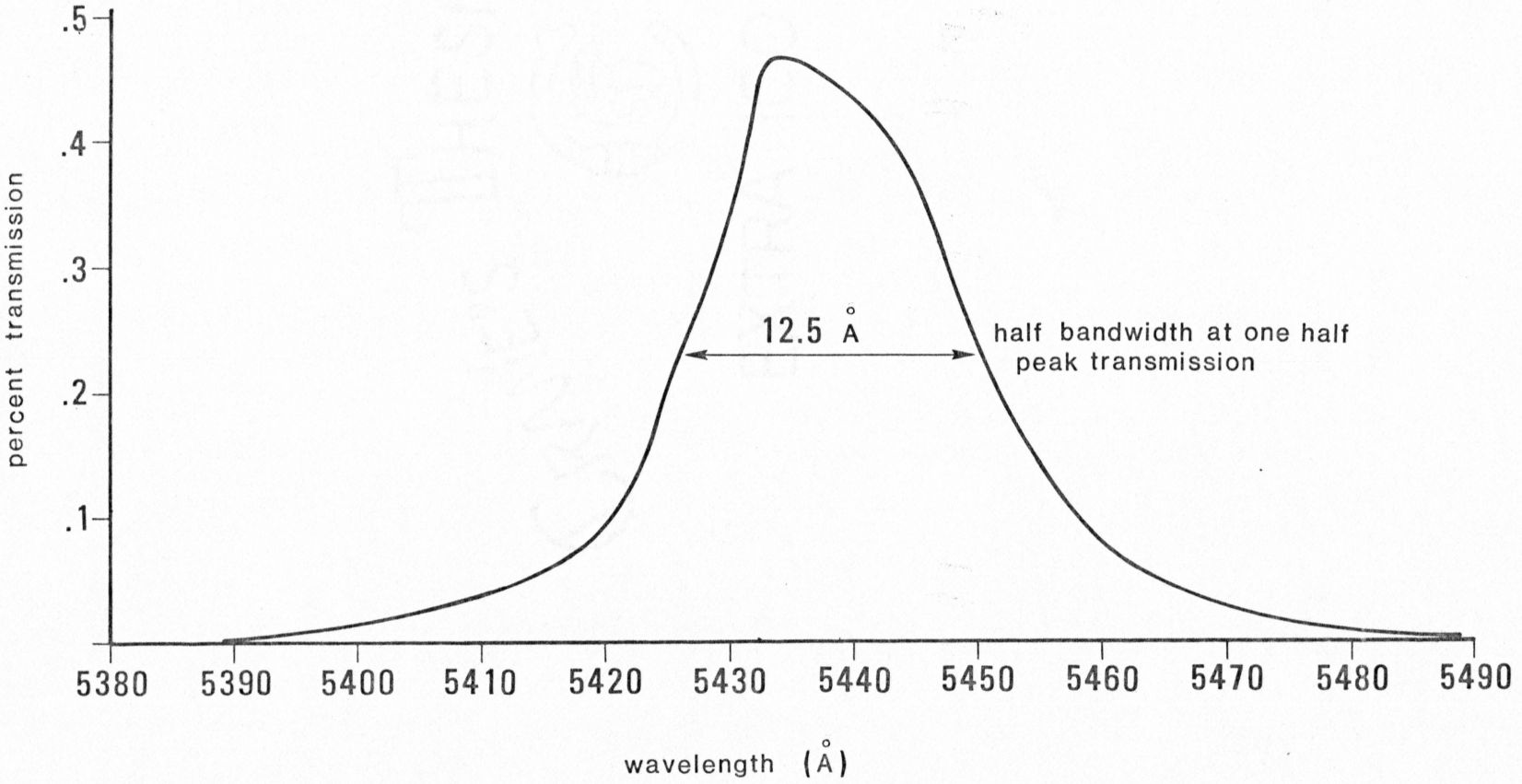

Fig. 3.2. Interference filter transmission curve

guard ring is made 100 volts positive. The current recorded is thus due to ions as well as secondard electron emission from both ions and neutrals.

The photomultiplier used was the RCA #7265 with an S-20 photocathode. The "typical" quantum efficiency of such a tube, specified by the manufacturer, is approximately 9% at 5436 Å. The cathode voltage used was 2.7 kV.

The photomultiplier detects a single photon by producing a small current pulse, which in turn produces a small voltage pulse across a suitable load. An R-C coupled preamplifier is used to amplify this voltage pulse at the output of the photomultiplier. The preamplifier output is then passed through a double delay line amplifier which increases the pulse height and shapes the pulse, a pulse height analyzer which further shapes and discriminates the pulses and finally to a counting scalar.

The counting system and the current integrator were simultaneously controlled by a timer which allowed the selection of a suitable integration period and permitted simultaneous integration of counts and secondary emission current. The current integration and pulse counting were started by a single switch and stopped when the timer reached a preset time (usually 1 minute).

Experimental Considerations

In order to obtain accurate values of the collision parameters from the measurement of beam current and signal, careful consideration has been given to the following:

1) Two collision processes: The theoretical expression in the previous section for fitting the experimental data was derived assuming that two collision processes producing the observed emission could be neglected. The useable pressure range for single collision conditions was estimated by measurements of the pressures at which the charge state of the ion beam showed the influence of two collision processes. If two collision processes began to make a significant contribution, the ion beam current failed to obey the solution of equation (2.3), corresponding to single collision conditions, i.e.,

$$I^+ = I_o^+ e^{-\sigma 10^n t^x}$$

Thus as long as $\ln (I^+/I_o^+)$ showed a linear dependence on pressure, single collision conditions were maintained. Whenever $\ln (I^+/I_o^+)$ departed from a linear dependence on pressure, two collision processes were beginning to contribute.

2) Scattering: The effect of scattering of a neutral beam was monitored by increasing the target pressure until there was a noticeable loss of beam current received at the Faraday cup. For the energy range form 8 to 24 keV, it was observed that there was no noticeable loss of beam current within the pressure range of the present experiment. Only at much higher target pressures (5×10^{-3} torr) did beam current begin to decrease. Thus in this range of energies, we may conclude that scattering of the beam is negligible. In the energy range of 4 to 7

keV, however, the effect of scattering became noticeable. At the highest target pressure (10×10^{-4} torr), the beam current decreased by approximately 30%. As long as the scattering occurs, however, before the beam reaches the photometer, the effect will be simply a proportional loss of both signal and beam current and the ratio of signal/I_s will be unaffected. It is reasonable to say that most of the scattering will take place either in chamber 1, due to the small entrance aperture, or in the target chamber, due to the much higher pressure encountered there. Scattering in chamber 3, between the photometer and the Faraday cup, will be taken up in part by the large dimension of the cup itself. We estimate that scattering in chamber 3 accounts for less than 5% of the total beam loss.

3) Contribution of extraneous emissions to the signal: In observing a particular emission, there must be no strong contaminating emissions near the wavelength of the emission being measured. If there is excitation by the beam of background N_2 gas, the N_2 first positive emission at 5442 Å must be considered as a possible contaminant to optical signal. However a study of signal versus observation chamber pressure clearly shows that the largest part of the signal must arise from beam atoms excited before entering the observation region. Furthermore, Figure 3.3 shows a typical auroral spectrum in the region of interest. The N_2 first positive (10,5) bandhead at 5442 Å is quite weak compared to the OI (6s-3p) line of interest. The contribution of the first positive system will be even weaker in the laboratory, since atoms are much less efficient in exciting the first positive system than auroral

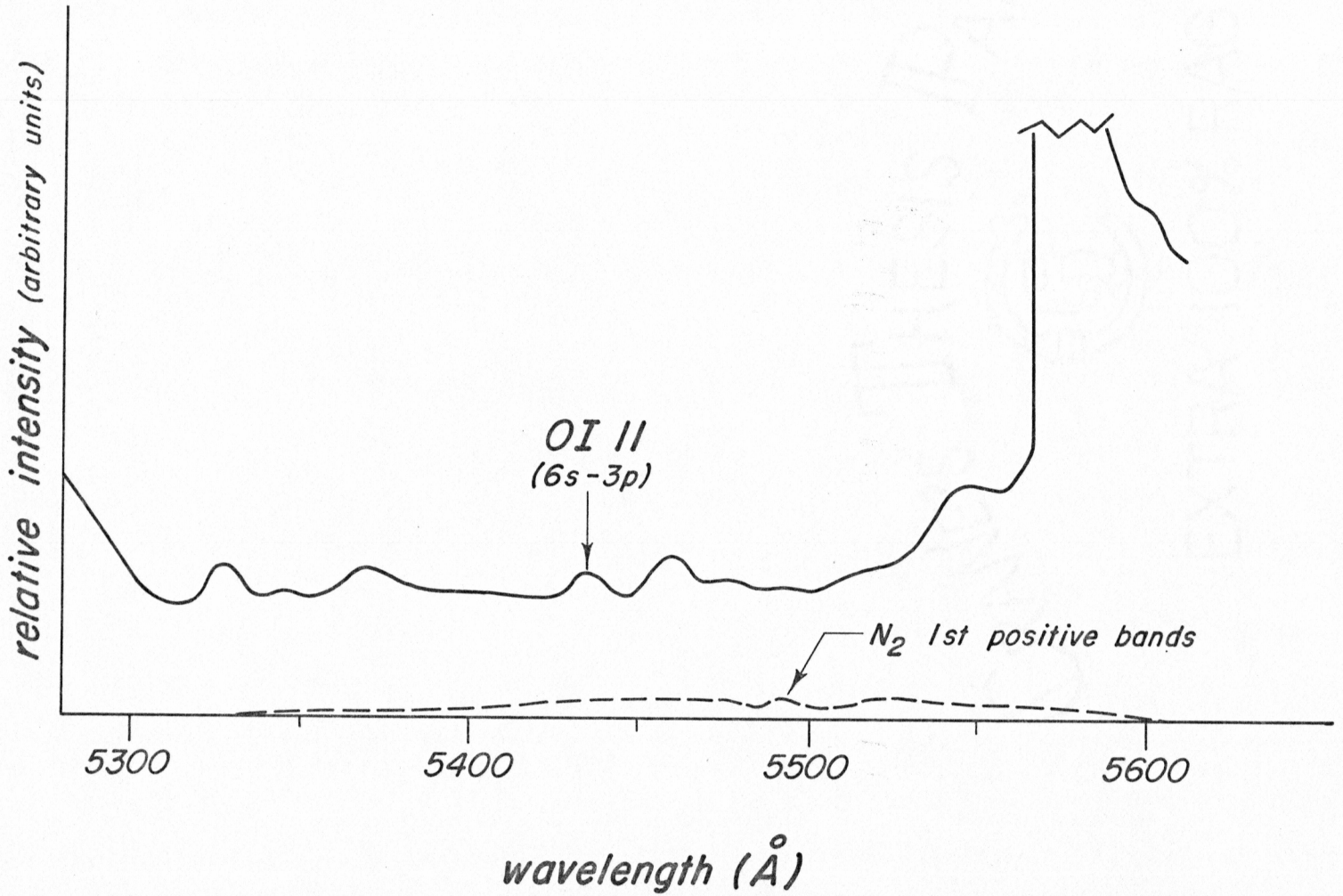

Fig. 3.3. Typical auroral spectrum in the region of interest

electrons. There are no emissions from N or N^+ that lie within the bandpass of the optical filter.

Also, any emission produced when the beam strikes the second collision chamber aperture must not reach the photomultiplier. This effect was prevented by placing the photometer in the observation chamber such that the exit aperture was not included in the field of view of the photometer. The entire viewing region was coated with colloidal graphite to eliminate reflections.

4) Polarization fraction: The emission produced in collisions of a beam with a target can sometimes be polarized. This results in anisotropy in the angular distribution of the resulting radiation. In many cases, this will affect the measurement of the absolute value for the excitation cross section. In the case of the 6s-3p transition observed in this experiment, however, little polarization and anisotropy in the radiation is likely to be present, since only the $3p\ ^5P_2$-$6s\ ^5S_2$ transition in the multiplet can be polarized and under many conditions this transition is also unpolarized.

The value for the deactivation cross section will also not be affected since this parameter depends only on the variation of signal with pressure.

Procedure

Having discussed the important considerations in the measurement of the observed signal, the experimental procedure will now be described.

Differential pressure between the collision chamber and the

reference chamber was measured with a capacitance manometer. Reference and observation chamber pressures were measured using ion gauges. The differential pressure is measured to within $\pm 0.2 \times 10^{-4}$ torr and the reference and observation chamber pressures are accurate to within 4×10^{-6} torr. Thus a typical target pressure of 2.5×10^{-4} torr is known to within ±10%.

a) Secondary emission coefficient, η: Measurements of the secondary emission coefficient as a function of energy were made in the energy range from 3 to 20 keV. Using a beam of O^+ ($I^o = 0$) and with no target gas present in the collision chamber, the currents I_i and I_{i+n} could be measured directly (I_i is the secondary emission current due to the impact of ions and I_{i+n} is the secondary emission current due to impact by both ions and neutrals). Equation (3.3) allows a straightforward calculation of η. The results of these measurements are shown in Figure 3.4.

b) Charge transfer cross section, σ_{10}: The charge transfer cross sections for electron capture by O^+ in collisions with N^2 were determined in a separate set of measurements. After mass analysis, an O^+ beam is passed through the target chamber. Here, no gas was admitted into the charge exchange cell and no deflecting voltage was applied. The beam will be composed of ions and a certain percentage of neutrals due to charge exchange. The ion current at any point along the beam path will be a function of pressure and distance travelled. Solving (2.3) for single collision conditions gives

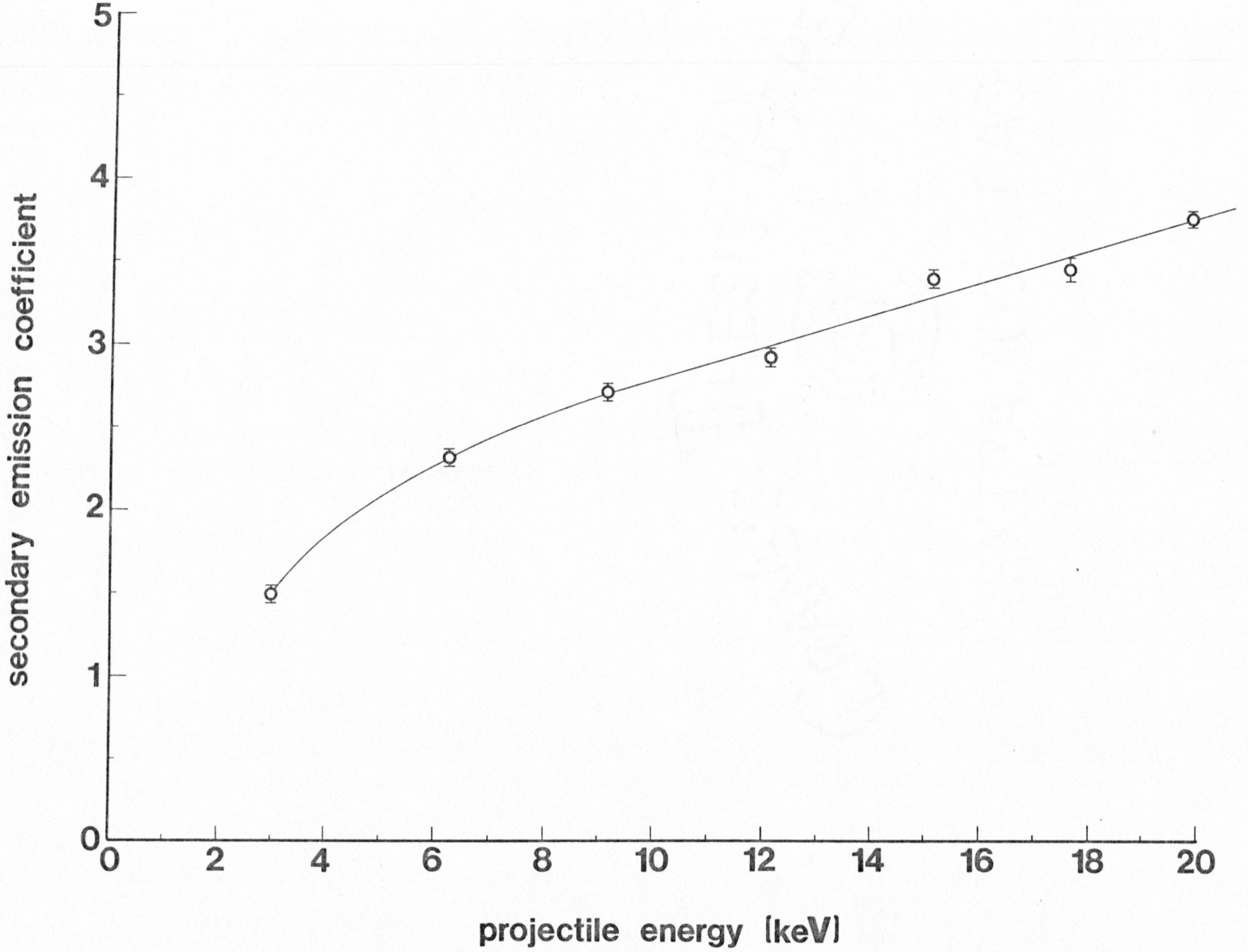

Fig. 3.4. Secondary emission coefficient vs. projectile energy

$$I_i = I_o^+ e^{-\sigma_{10} n_t x} \tag{3.1}$$

where I_o^+ is the ion current at $x = 0$, σ_{10} is the charge transfer (also called electron capture) cross section and n_t is the target number density. This expression can be written as

$$\ln \frac{I_i}{I_o^+} = -\sigma_{10} n_t x \tag{3.2}$$

The current I_{i+n} from secondary electrons produced by the beam plus the current from the ions themselves is given by

$$I_{i+n} = \eta(I^o + I_i) + I_i \tag{3.3}$$

where I_i and I^o are ion and neutral "currents" respectively, and η is the secondary emission coefficient. By definition $I_o^+ = I^o + I_i$. Solving this latter relation for I^o, substituting into (3.3) and rearranging terms gives

$$I_o^+ = \frac{I_{i+n} - I_i}{\eta} \tag{3.4}$$

Dividing by I_i, inverting and taking the natural logarithm of both sides

yields

$$\ln \left(\frac{I_i}{I_{i+n} - I_i}\right) = \ln \left(I_i/I_o^+\right) - \ln \eta \qquad (3.5)$$

Replacing $\ln (I_i/I_o^+)$ by (3.2) yields

$$\ln \left(\frac{I_i}{I_{i+n} - I_i}\right) = -\sigma_{10} n_t x - \ln \eta \qquad (3.6)$$

This can also be expressed as

$$\ln \left(\frac{I_{i+n} - I_i}{I_i}\right) = \sigma_{10} n_t x + \ln \eta \qquad (3.7)$$

We can write $n_t x$ as a sum over each of the pressure regions, i.e., $\Sigma n_i x_i = 3.152 \times 10^{12} \Sigma p_i x_i$. This sum is expressed in torr-cm and is termed the "effective path" of the beam. Graphing $(I_{i+n} - I_i)$ versus $\Sigma p_i x_i$ on semilog paper yields a slope proportional to σ_{10} and an intercept $\ln \eta$. N_2 target pressures ranged from 0 to 5×10^{-4} torr. All data was linear within this range, which insured single collision conditions. The slope was obtained from a visual best fit to the data. The measured currents are recorded together to eliminate variations of beam current time. Note that σ_{10} may be found without knowledge of the secondary emission coefficient. Figure 3.5 shows a sample plot of the

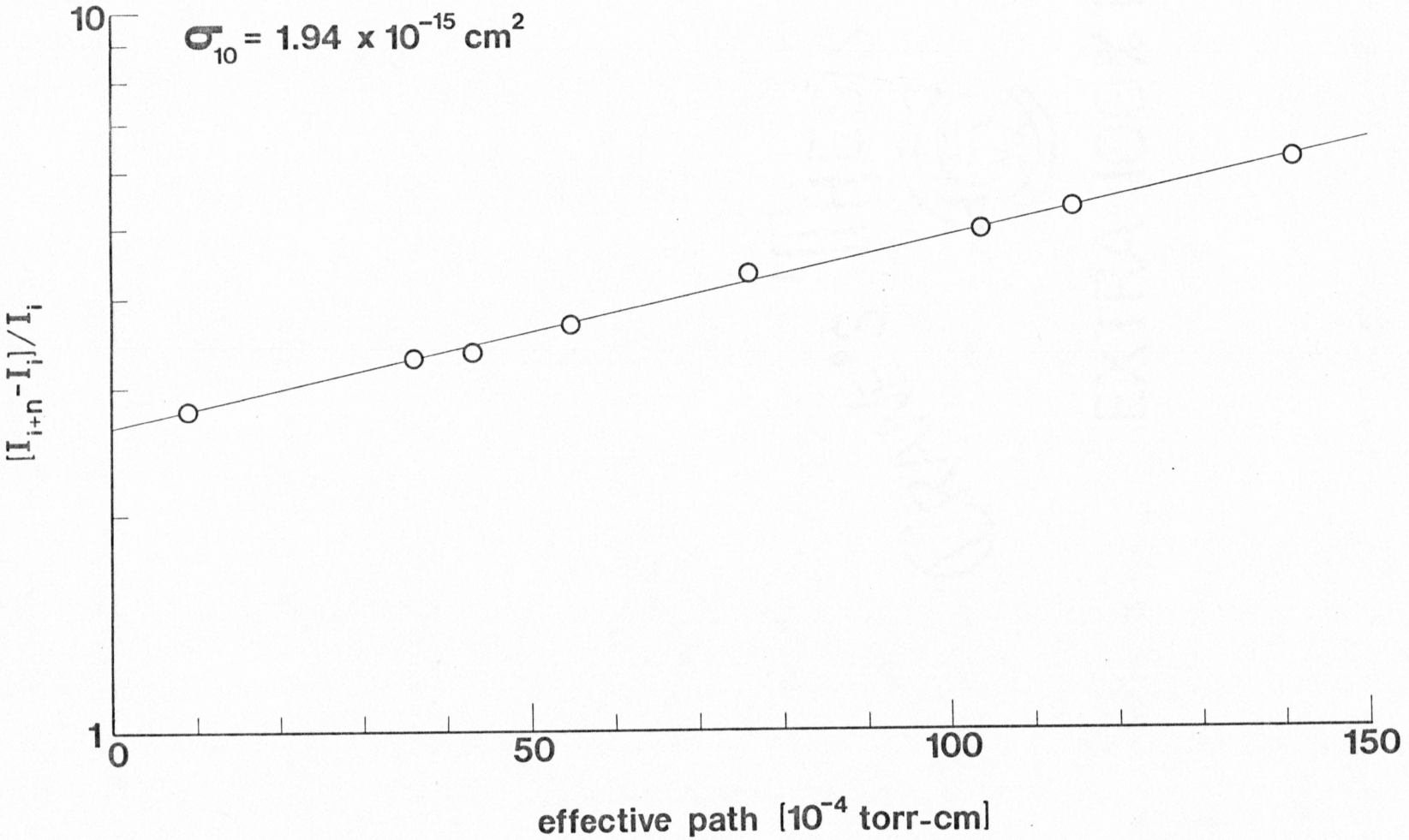

Fig. 3.5. Sample plot of ln $(I_{i+n} - I_i)/I_i$ vs. effective path for determining charge transfer cross section

data for 8.7 keV O^+ ions in N_2.

c) Deactivation cross section: A beam of mass analyzed O^+ ions undergoes charge exchange, forming neutral O (approximately 50% of the incident O^+). The remaining O^+ is deflected and the resultant neutral beam is passed through the collision chamber, producing the observed signal. The beam is received by the Faraday cup at the end of the observation chamber. As has been shown, the neutral beam current remains undiminished over the range of pressures used in this experiment. The neutral beam flux at the point of observation is thus the same as its initial value.

The optical signal was measured by subtracting the dark counts from the signal plus dark counts. The dark counts were measured during two, one minute intervals when the beam was removed from the viewing region by changing the beam energy before it passed through the mass analyzer. The signal plus dark counts were recorded with the beam passing through the target gas during a one minute interval between the two dark count readings. The oscillator and magnet were kept in operation throughout this procedure to reduce possible effects of magnetic field and r-f pickup. The signal was computed by subtracting the average of the two dark count readings from the signal plus dark counts. The photomultiplier was not cooled and dark counts ranged approximately between 800 and 1000 counts per second. High voltage was constantly applied to the tube, including periods when the equipment was not in use. This insured a more stable response of the photomultiplier and minimal dark counts. Signals ranged from 0 to 100 counts per second.

The data used to fit equation (2.20) consisted of average values of signal/I_s for several runs, taken at equally spaced intervals in the target pressure range from 0 to 10 x 10^{-4} torr. For each value of target pressure (p_2), the pressures in the reference chamber (p_1) and observation chamber (p_3) were also measured.

The numerical value for the deactivation cross section was determined by an iterative computer program (see appendix), which determines the least squares fit of equation (2.20) to the experimental values for signal/I_s, p_1, p_2, and p_3. Iterations in the program continued until the correction in the value for each parameter was significantly less than 1%. An example of the data points and the resulting best fit is shown in Figure 3.6. One of the two unknown parameters is σ_d. It is the source of the overall curvature of the data. The other unknown parameter, B, is defined as

$$B = \frac{\eta_{6s} A_{ij} L\sigma^*}{ev\eta} \qquad (3.8)$$

which is proportional to the excitation cross section. Recall that the term involving parameter A (= $\eta_{6s} A_{ij} Lf^*/ev\eta$) was found to be negligible. The term $1/v\tau$ used in the program was calculated by determining the velocity from the measured kinetic energy for a beam of atomic oxygen; the lifetime of the excited state is the value reported by Weise et al. of .328 μsec.

d) Absolute calibration for the excitation cross section: The numerical value of the cross section for excitation of O into the state

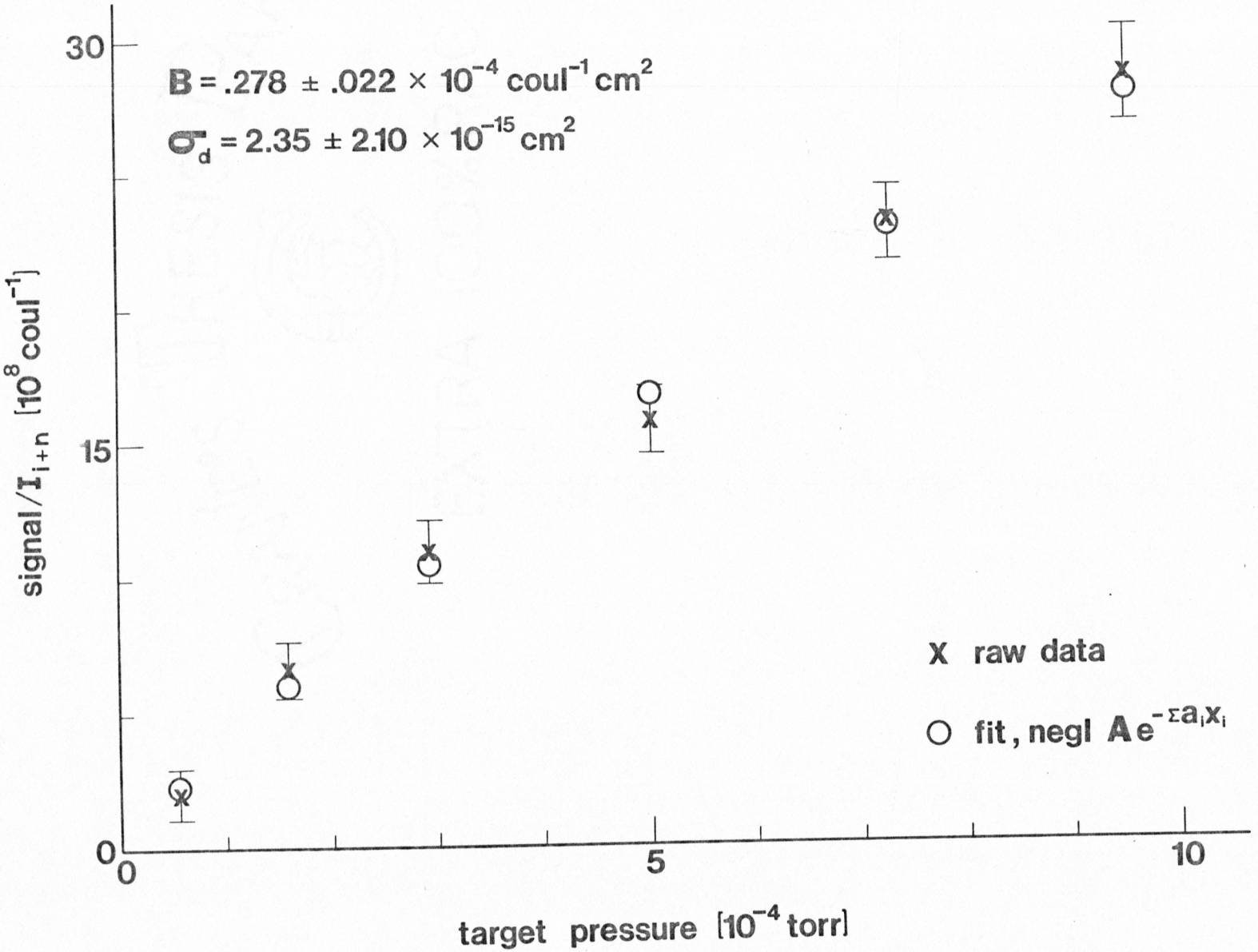

Fig. 3.6. Sample plot of signal/I_s vs. target pressure for determining deactivation cross section

of interest was determined by an absolute calibration of the overall detection efficiency of the system. The signal, beam current and N_2 target pressure were monitored for a beam of H^+ at an energy of 5.85 keV. The observed optical emission was H_α(6563 Å). A calculation of the quantity (signal/I_i)n_t (where I_i is the ion beam current and n_t is the target gas number density) and the previous results of Succhanek (1974) for the H_α excitation cross section at this energy, allowed a determination of η_α, the overall efficiency of the detection system at 6563 Å (using a specified Barmer α interference filter). Using this result and a knowledge of the relative overall efficiencies at 6563 Å and 5436 Å, σ^* can be determined from the parameter B (equation 3.8).

From the definition of the cross section

$$\sigma \equiv \frac{\text{\# of events/time}}{\text{incident flux density x \# targets}} \tag{3.9}$$

The flux density is just nv, where n is the number density of ions in the beam and v is the velocity. Since beam current is nevA and since the number of targets is just nV, where V is the volume, we can solve (3.9) as follows:

$$\text{\# of events/time} = \sigma n l \, (I_i/e) \tag{3.10}$$

But the number of events/time is just the observed signal divided by the overall efficiency of the system. Thus for H_α

$$\frac{\text{signal}}{\varepsilon_\alpha T_\alpha} = \sigma_\alpha nL\ (I_i/e) \tag{3.11}$$

where α subscripts correspond to the H_α emission. Here $\eta_\alpha = \varepsilon_\alpha T_\alpha$ is the overall efficiency at H_α. ε_α is the overall efficiency of the system, without a filter, at 6563 Å and T_α is the percent transmission of the H_α filter at 6563 Å. Equation (3.11) becomes

$$\varepsilon_\alpha T_\alpha L = \frac{\text{signal}}{I_i n}\ (e/\sigma_\alpha) \tag{3.12}$$

Using a value for σ_α of 7×10^{-18} cm^2 at 5.85 keV (Succhanek, 1974) and the experimental values for (signal, $I_i)n_t$, it was found that $\varepsilon_\alpha T_\alpha L = 1.118 \times 10^{-4}$ cm. The overall efficiency, η_{6s}, for the 5436 Å emission can be related to that for H_α using

$$\eta_{6s} = \varepsilon_{6s} T_{6s} = \varepsilon_\alpha T_\alpha \left(\frac{T_{6s}}{T_\alpha}\right)\left(\frac{\varepsilon_{6s}}{\varepsilon_\alpha}\right) \tag{3.13}$$

Subscripts 6s refer to the (6s-3p) transition. Values for T_α and T_{6s} are known from the filter curves (32% and 40% respectively) and the ratio $\varepsilon_{6s}/\varepsilon_\alpha$ is determined from the spectral characteristics of the S-20

photocathode. The latter ratio is 9.3/4. Using these values, and noting that L is the same for H_α as for the present experiment, one obtains $\eta_{6s}L = 3.249 \times 10^{-4}$ cm. Returning now to equation (3.8) and solving for σ^*, we have

$$\sigma^* = (ev\eta/\eta_{6s}A_{ij})B \tag{3.14}$$

σ^* was first calculated at an energy of 12.8 keV, substituting the known values for B ($.101 \times 10^{-4}$ $coul^{-1}$ cm^2), η (3.1) and v (3.92×10^7 cm/sec). It was found at that energy that $\sigma^* = 1.98 \times 10^{-19}$ cm^2. The cross section for excitation at other energies can then be calculated using the values of B(E), η(E) and v(E) for each energy, i.e.,

$$\sigma^*(E) = \frac{B(E)}{.101 \times 10^{-4}} \times \frac{\eta(E)}{3.1} \times \frac{v(E)}{3.92 \times 10^7} \times 1.98 \times 10^{-19} \text{ cm}^2$$

4. RESULTS AND DISCUSSION

Charge transfer cross section

The results of our measurements of the charge transfer cross sections for the reaction $O^+ + N_2 \rightarrow N_2^+ + O$ as a function of the O^+ beam energy are shown in Figure 4.1 with an accompanying best fit curve to the data. In the lower energy range, the cross section rises linearly from 1.22×10^{-15} cm^2 at 3.0 keV tO 1.94×10^{-15} cm^2 at 8.7 keV. Extrapolation of the curve into the thermal energy range gives a cross section of $.53 \times 10^{-15}$ cm^2. Beyond 10 keV, the curve flattens, reaching a maximum near 2.31×10^{-15} cm^2 at an energy of about 20 keV. Beyond 20 keV, the cross section decreases slightly to 2.28×10^{-15} cm^2 at 25 keV. The uncertainty in the values of the cross sections are relatively small. Estimates of the overall error in σ_{10} were made by estimating the uncertainty in the slope of the data and the error in the pressure readings. The error due to fitting a straight line to the data is relatively small since fluctuations of $(I_{i+n} - I_i)/I_i$ over the whole pressure range were small. Uncertainty in the pressure readings becomes significant only at the lowest pressures. We estimate the overall error in the values of σ_{10} to be ±6%.

Several important factors must be considered in an interpretation of the present results as well as comparisons of these results with those of other authors. Consideration must be given to the presence of NO^+ in the beam resulting from atom interchange ($O^+ + N_2 \rightarrow NO^+ + N$). A number of workers have studied this reaction at thermal energies and

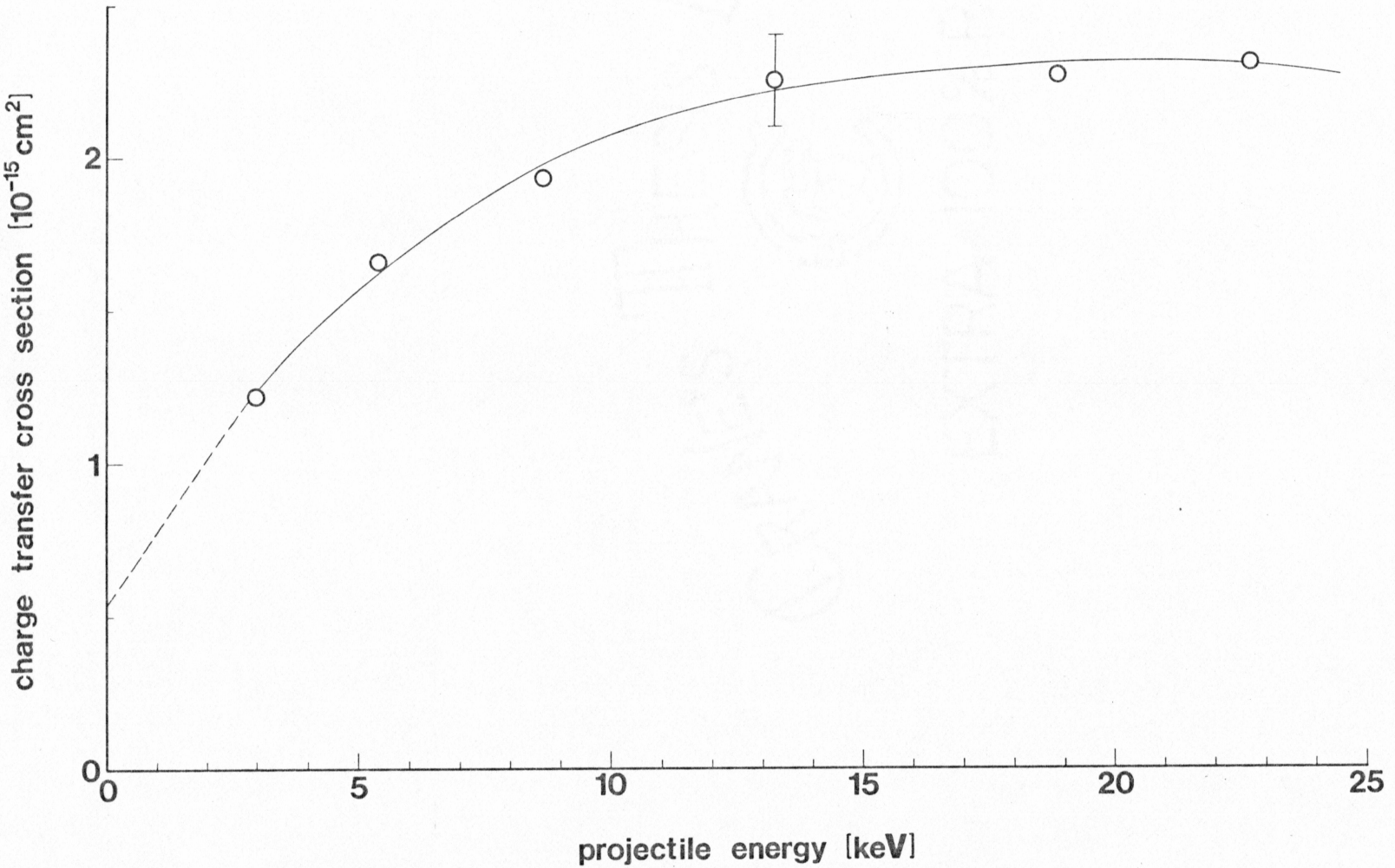

Fig. 4.1. Charge transfer cross section vs. projectile energy

for different vibrational levels of N_2. Kosmider and Hasted (1975) show the cross section for this reaction to be increasing out to .5 ev ($.25 \times 10^{-16}$ cm^2). Johnsen and Biondi (1973) measured reaction rates for NO^+ production and extended the energy range to 1.2 ev. Measurements over a wider range of energies, however, reveal that the cross section reaches a maximum and falls off at higher energies. Cohen (1972), using a modulated cross beam apparatus, measured the cross section for $O^+ + N_2 \rightarrow NO^+ + N$ at energies 4 to 26 ev. The N_2 temperature was varied from 1000 to 3000 ^oK to obtain the different vibrational levels. The cross section was found to rise to a value of 5×10^{-16} cm^2 at near 14 ev and decrease to 1×10^{-16} cm^2 at near 26 ev. This decrease was shown to be nearly independent of the N_2 temperature. Neynaber and Magnuson (1972) used a merging beam apparatus for O^+ energies to 15 ev. Their cross sections were termed "relative," being averaged over both ground and excited states of O^+ and N_2. They show a decreasing cross section beyond 5 ev. Their results also demonstrate that the forward scattering of NO^+ decreases with increasing beam energy. The presence of N_2 vibrational levels does not greatly affect the cross section for NO^+ production, which is in agreement with Cohen. A semi-empirical model for this reaction was devised by O'Malley (1969) for any combination of O^+ energies and N_2 temperatures. This model, in general agreement with the experimental results, shows a peak at around 8 ev and decreasing at higher energies. From these results we conclude that both production and forward scattering of NO^+ is insignificant in the energy range 3 to 25 keV, and that the current measured in the

present study is due solely to O and O^+ in the reaction $O^+ + N_2 \rightarrow O + N_2^+$.

The observed charge transfer cross section will depend upon the fraction of excited states present in the O^+ beam. Hughes and Tiernan (1971) showed that this fraction, in turn, depends upon the gas used as the source of O^+. This fraction varies from .038 when CO_2 is used in the source to .95 for H_2O. The fraction for O_2 (present experiment) has been determined accurately at .28 (Turner et al.). This variation in O^{+*} will affect the measurements of σ_{10}. Any comparison, therefore, of the results of charge transfer for the reaction $O^+ + N_2 \rightarrow N_2^+ + O$ (or any similar reaction) can be made only for beams of incident ions which have nearly the same fraction of excited states.

Previous measurements of charge transfer for $O^+ + N_2 \rightarrow N_2^+ + O$ have been made for several ranges of energies. Potter (1954) found σ_{10} to be fairly constant ($.5 \times 10^{-15}$ cm^2) between 9 and 250 ev, in close agreement with our extrapolated value for E = 0 of $.53 \times 10^{-15}$ cm^2. Ormrod and Michel (1971) measured σ_{10} in the energy range 15-90 keV. Their results show a slow rise in σ_{10} from 2.7×10^{-16} cm^2 at 15 keV to a maximum near 5.7×10^{-16} cm^2 at 60 keV. These values lie consistently below those of the present experiment. However, the validity of their results is somewhat in doubt. Target pressures ranged as high as 10^{-3} torr, well beyond the useable pressure range we observed for single collision conditions. Also, the expression the authors used as a beam equilibrium equation seems to be in error in the second term of an expansion, which would lead to anomolously low values for σ_{10}. The work

of Stebbings et al. (1962) and Solove'v et al. (1972) yielded cross section measurements in energy ranges above and below that of the present experiment. In both cases, the experimental procedure was similar to ours, in which monoenergetic beams of O^+ ions underwent charge exchange with N_2. The resulting neutral beam interacted with an N_2 target. In both cases, pure O_2 was used in the ion source. The results are in good agreement with those of the present work (Figure 4.2). Stebbings et al. (1962) found σ_{10} to rise slowly from near 8×10^{-16} cm^2 at 1 keV to 1×10^{-15} cm^2 at 4.9 keV. Solove'v et al. (1972) measured σ_{10} in the 28-180 keV range. They observed the cross section to decrease from 1.25×10^{-15} cm^2 at 28 keV to 6×10^{-16} cm^2 at 180 keV. All measurements of σ_{10} presented here are "composite" cross sections, i.e., cross sections that include contributions due to all the various excited states of O^+ and all vibrational levels of the N_2 target. Our results are consistent with Stebbings et al. (1962) in the narrow region of overlap in the data from 3 to 5 keV. At 1 keV, an extrapolation of our curve gives σ_{10} near 8×10^{-16} cm^2, again in close agreement. There is no energy overlap between the results of Solove'v et al. (1972) and those of the present experiment. However, the data of Solove'v et al. (1972) is still rising (1.25×10^{-15} cm^2 at 28 keV) and indicates a maximum below this energy. This is in reasonable agreement with the results of the present experiment, which show a maximum cross section of 2.3×10^{-15} cm^2 at near 20 keV. All results in this region are consistent with the "adiabatic criterion." For the reaction $O^+ + N_2 \rightarrow N_2^+ + O$, if one uses the energy for the maximum cross section observed in our experiment (20 keV), the

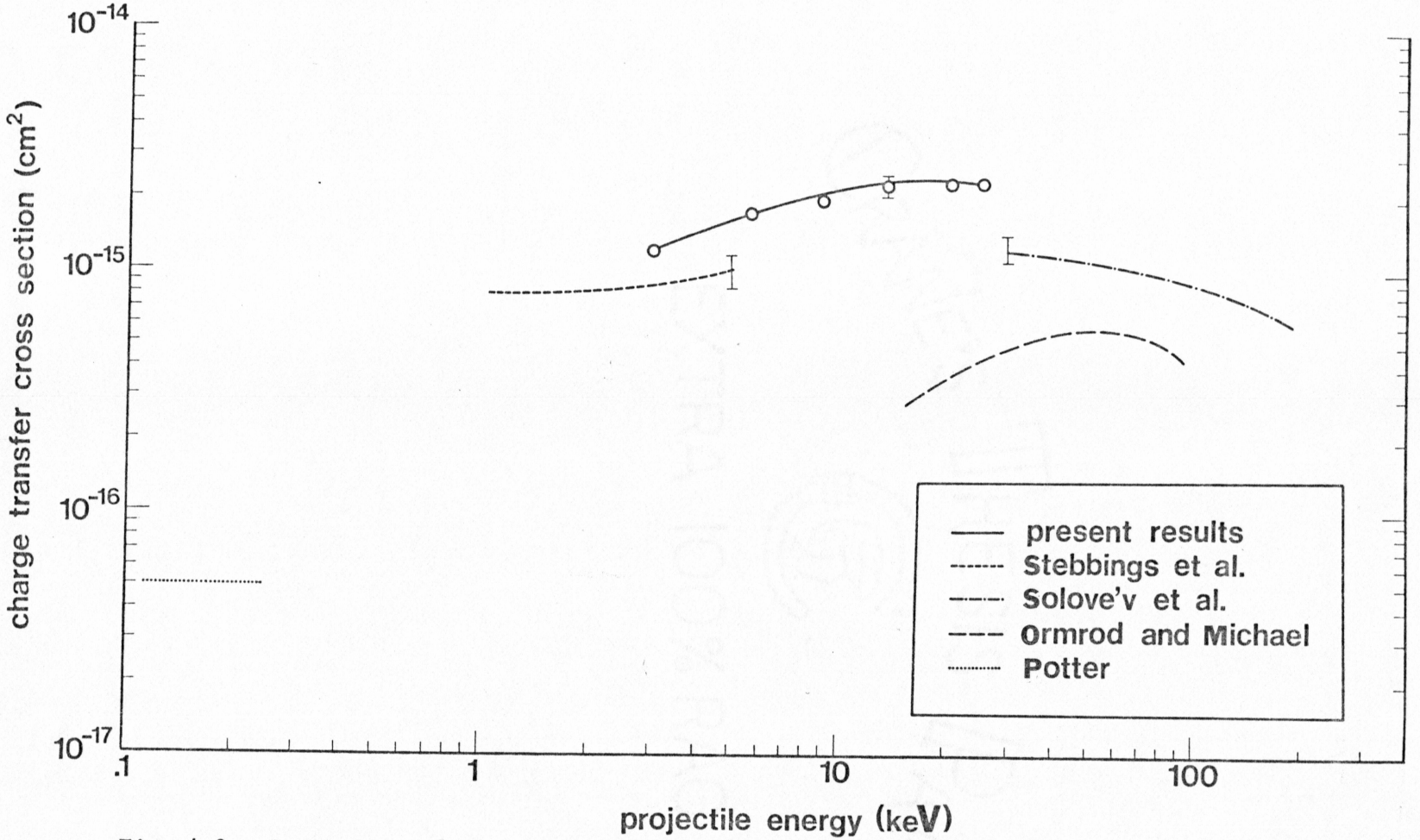

Fig. 4.2. Comparison of charge transfer cross sections vs. projectile energy in present experiment to other authors

adiabatic criteron yields an effective range (interaction distance) of 1.05×10^{-7} cm, which agrees well with that normally used for such collision reactions.

Finally, one stripping cross section measurement was made at an energy of 20 keV. Our result was $\sigma_{01} = 1.37 \times 10^{-16}$ cm^2. This compares to a value of 1.3×10^{-16} cm^2 measured by Solove'v et al. (1972) at an energy of 28 keV. Our measurement at 20 keV gives a value for $g/f = \sigma_{10}/\sigma_{01} = 16.8$ compared to the value of 74.4 measured at 10 keV, showing a sharp increase in this ratio from 20 keV to 10 keV.

Deactivation and excitation cross section

The values obtained for deactivation and excitation cross sections are presented in Figures 4.3 and 4.4. Values of the parameters B and σ_d in equation (2.20) were determined in as many as 5 different measurements for a given energy. Each of these measurements, as described earlier, consists of a fit of the beam dynamic equation to as many as 35 separate data points, depending on the magnitude of the signal. The average values form a smooth curve in spite of a scatter in the separate values. This scatter is consistent with the error estimates for the parameters. Both deactivation and excitation cross sections show a similar behavior, rising toward lower energies. The deactivation cross section is fairly constant (near 1.5×10^{-15} cm^2) in the energy range 11-19.6 keV, but rises to near 7×10^{-15} cm^2 at an energy of 4 keV. Excitation cross sections also remain nearly constant around 2.25×10^{-19} cm^2 from 10 to 19.6 keV, but rise in similar fashion to 3.25×10^{-19} cm^2 at 4 keV. There is a large variation in the estimated uncertainty in

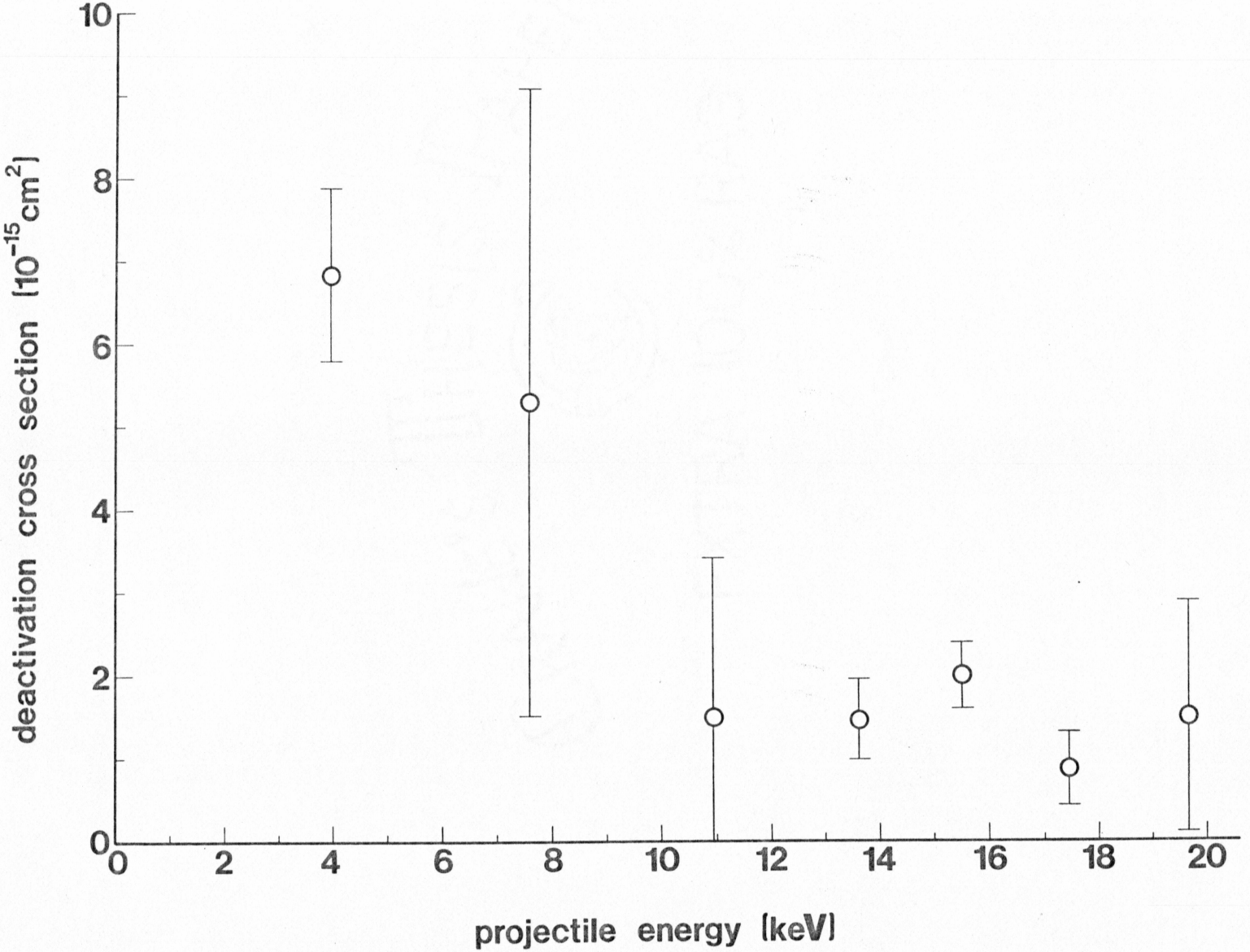

Fig. 4.3. Deactivation cross section vs. projectile energy

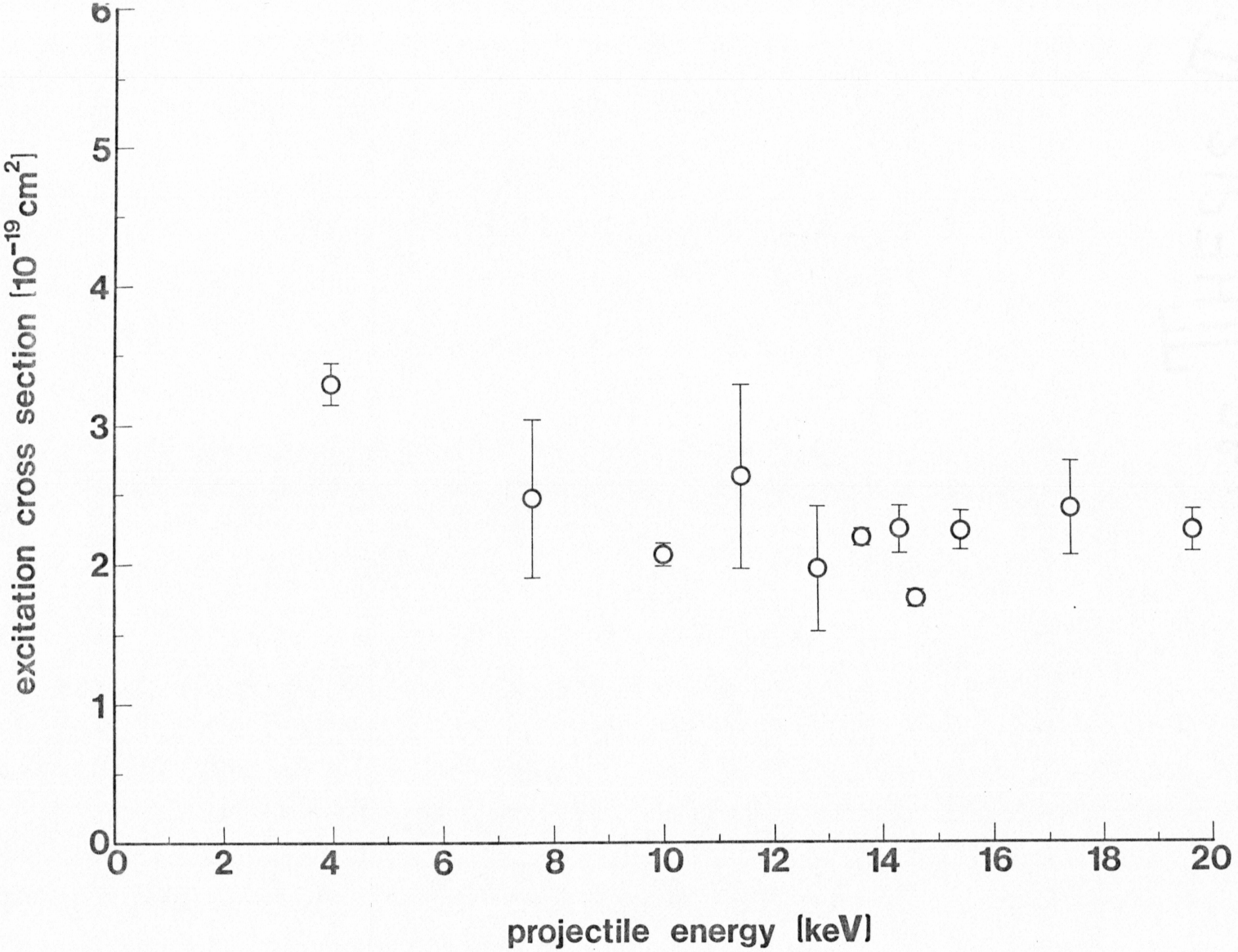

Fig. 4.4. Excitation cross section vs. projectile energy

different values of both cross sections. The main source of the large uncertainty in the deactivation cross section at low energy results from large fluctuations in signal/I_{i+n}. At these low energies the beam currents were small and generally less stable. The error shown, where results are averages of more than one measurement, is the standard deviation of the mean for these measurements. At higher energies, where signals were large enough so that only one measurement was required, the error shown is the largest of (1) the error calculated from scatter in the experimental data for signal/I_{i+n} at a given pressure or (2) error calculated from scatter of the averaged data for signal/I_{i+n} from the computer fit. Pressure readings are accurate to within 4×10^{-6} torr. In addition to the random errors shown for the cross sections, systematic error also introduces an uncertainty in the value of σ_d. The following is a list of possible systematic errors leading to uncertainty in σ_d in the present experiment:

1) error in pressure measurements due to error in calibration of ion gauges

2) error in the reported transition probability of the 6s-3p transition

3) contributions from $A\Sigma e^{-\alpha_i x_i}$, neglected in the theorectial expressions for signal/I_{i+n}

4) target gas excitation

5) error in determination of the beam velocity

The uncertainty in the absolute value for the beam energy is ±.25 keV with a reproducibility of ±.05 keV. We estimate a random error of ±25% and an overall uncertainty in the values of σ_d of ±35%.

In the case of the excitation cross section, the effect of random error is smaller than in the results for σ_d. We estimate the overall random error to be ± 11%. However, the absolute calibration of the optical detector is probably no more accurate than ±20%. In addition, error in the determination of the secondary emission coefficient, as well as the systematic errors listed above increase the uncertainty in the values of σ^*. We thus estimate the overall uncertainty in the reported values of σ^* to be ±25%.

No comparisons with previous work can be made, since there have been no other measurements made of σ^* and σ_d for the 6s-3p transition of neutral oxygen at any energy. In briefly discussing our results, we note the similarity in the curves of Figures 4.3 and 4.4, decreasing at higher energies and rising sharply below 8 keV. This behavior indicates a stronger interaction between O and N_2 at low energies, where the process of excitation and deactivation are both enhanced. This in turn implies a curve crossing, which is useful in a qualitative way in demonstrating how certain nonresonant reactions can proceed rapidly at thermal energies.

The importance of collisional deactivation of the 6s ^5S state of neutral oxygen in the upper atmosphere can be assessed by comparing the relative contributions of the terms $\sigma_d n_t$ and $1/v\tau$ that appear in the theoretical expressions in section 2. The table below presents a comparison of the contributions of $\sigma_d n_t$ and $1/v\tau$ over a range of altitudes and corresponding atmospheric number densities. The value of σ_d is the cross section at 3.85 keV (6.84×10^{-15} cm^2). At this energy, v = 2.15

x 10^7 cm/sec. τ is the lifetime of the 6s ^{5}s state mentioned earlier, i.e., .328 μsec.

altitude (km)	number density (cm^{-3})	$\sigma_d n_t$	$1/v\tau$
75	8.616×10^{14}	5.89	.142
80	3.462×10^{14}	2.37	.142
90	7.007×10^{13}	.479	.142
100	1.070×10^{13}	.073	.142
110	1.835×10^{12}	.013	.142

Thus at altitudes below 80 km., the number density is great enough that collisional deactivation dominates. From 80 to 110 km., the two processes are competitive. At altitudes greater than 110 km., the number density is small enough that radiative decay will dominate.

5. Conclusion

Absolute collisional deactivation and excitation cross sections were obtained for a beam of neutral atomic oxygen incident on a target gas of N_2. These are the first cross sections measured for the 6s - 3p transition of neutral oxygen at any energy.

The cross sections for charge transfer of a beam of singly ionized oxygen incident on N_2 were also measured in an energy range previously unexplored. The results fit well in between values measured by other authors in energy ranges above and below that of the present experiment.

The agreement of the present results with those of other authors is a demonstration of the success of this new technique for cross section measurements. In this technique, the optical signal from a desired transition is isolated from the interaction of a beam of specified energy and a target gas. This variation in signal is recorded as a function of target gas pressure, and values for these are fitted to a beam growth equation. A best fit of the data yields both the excitation and deactivation cross sections, which are parameters in the equation.

The results and technique presented here encourage a further investigation of a variety of beam-target interactions in the 3-20 keV range. The cross sections obtained find one important application in auroral modeling, where energies and pressures are the same as those simulated in the laboratory. Cross sections play an essential part in any atmospheric model to enhance and help complete an understanding of those complex processes occuring in the upper atmosphere.

APPENDIX

DATA ANALYSIS PROGRAM

```
10  REM  DELETE LINES 80-110 FOR ALL BUT BEAM ANALYSIS PROGRAMS
20  REM  STORE DATA TEMPORARILY IN FILE T
30  REM  FOR YI=F(XI(J)) DATA FILE IS:  X1(1), X1(2),...,Y1,W1,X2(1),
31       & X2(2),...ETC.
40  REM  WI ARE WEIGHTING FACTORS, I.E. NUMBERS PROPORTIONAL TO
41       & 1/(ERROR)↑ 2
50  REM  PARAMETERS ARE A,B,C,D AND E: IN THE PROGRAM THEY ARE P(1)
51       & THRU P(5)
60  REM  ENTER SUBROUTINE FOR THE FUNCTION AND PARTIAL DERIVATIVES AT
61       & 1200
70  REM  PARTIAL WITH RESPECT TO ITH PARAMETER IS F2(I), FUNCTION IS F1
80  PRINT "ENERGY(KEV),MASS(AMU),LIFETIME(SEC),X1,X2, AND X3(CM)"
90  INPUT E,M1,T,X1,X2,X3
100  R=4.38E7*T*SQR(E/M1)
110  PRINT "1/VT" IS "1/R" AND VELOCITY IS "R/T"
120  FILES T
130  PRINT "# PARAMETERS, # DATA, # INDEPENDENT VARIABLES"
140  INPUT M,N,D
150  FOR I=1 TO M
160  PRINT "GUESS FOR PARAMETER" I
170  INPUT P(I)
180  NEXT I
190  MAT A=ZER(M,M)
200  MAT B=ZER(M,M)
210  MAT C=ZER(M,M)
220  MAT D=ZER(M,M)
230  MAT E=ZER(M,M)
240  MAT F=ZER(M,M)
250  FOR I=1 TO N
260  FOR J=1 TO D
270  INPUT #1,X(J)
280  NEXT J
290  INPUT #1,X(J)
300  GOSUB 1200
310  Z=Y-F1
320  FOR K=1 TO M
330  FOR L=1 TO M
340  IF L=1 THEN 370
350  A(K,L)=F2(K)*F2(L)*W+A(K,L)
360  GO TO 380
370  A(K,1)=Z*F2(K)*W+A(K,1)
380  IF L=2 THEN 410
390  B(K,L)=F2(K)*F2(L)*W+B(K,L)
400  GO TO 420
```

```
410  B(K,2)=Z*F2(K)*W+B(K,2)
420  D(K,L)=F2(K)*F2(L)*W+D(K,L)
430  IF M=2 THEN 580
440  IF L=3 THEN 470
450  C(K,L)=F2(K)*F2(L)*W+C(K,L)
460  GO TO 480
470  C(K,3)=Z*F2(K)*W+C(K,3)
480  IF M=3 THEN 580
490  IF L=4 THEN 520
500  E(K,L)=F2(K)*F2(L)*W+E(K,L)
510  GO TO 530
520  E(K,4)=Z*F2(K)*W+E(K,4)
530  IF M=4 THEN 580
540  IF L=5 THEN 570
550  F(K,L)=F2(K)*F2(L)*W+F(K,L)
560  GO TO 580
570  F(K,5)=Z*F2(K)*W+F(K,5)
580  NEXT L
590  NEXT K
600  NEXT I
610  MAT R=INV(A)
620  C1=DET(X)
630  MAT R=INV(B)
640  C2=DET(X)
650  MAT R=INV(D)
660  C6=DET(X)
670  P6=C1/C6
680  PRINT "CHANGE IN A=" P6
690  P(1)=P6+P(1)
700  PRINT "A=" P(1)
710  P7=C2/C6
720  PRINT "CHANGE IN B=" P7
730  P(2)=P7+P(2)
740  PRINT "B=" P(2)
750  IF M=2 THEN 960
760  MAT R=INV(C)
770  C3=DET(X)
780  P8=C3/C6
790  PRINT "CHANGE IN C=" P8
800  P93)=P8+P(3)
810  PRINT "C=" P(3)
820  IF M=3 THEN 960
830  MAT R=INV(E)
840  C4=DET(X)
850  P9=C4/C6
860  PRINT "CHANGE IN D=" P9
870  P(4)=P9+P(4)
880  PRINT "D=" P(4)
890  IF M=4 THEN 960
900  MAT R=INV(F)
```

```
910  C5=DET(X)
920  P3=C5/C6
930  PRINT "CHANGE IN E=" P3
940  P(5)=P3+P(5)
950  PRINT "E=" P(5)
960  PRINT "TO CONTINUE, ENTER 1; TO STOP ENTER ANY OTHER #"
970  INPUT T
980  RESTORE #1
990  IF T=1 THEN 190
1000  FOR I=1 TO N
1010  FOR J=1 TO D
1020  INPUT #1,X(J)
1030  NEXT J
1040  INPUT #1,Y,W
1050  GOSUB 1200
1060  PRINT "FOR DATA POINT "I" FUNCTION IS" F1
1070  Z=Y-F1
1080  FOR J=1 TO M
1090  S1(J)=W*(Z/F2(J))↑ 2+S1(J)
1100  R1(J)=1/F2(J)↑ 2+R1(J)
1110  NEXT J
1120  S2=W+S2
1130  NEXT I
1140  FOR J=1 TO M
1150  PRINT "FIT ERROR IN PARAMETER "J" IS" SQR(S1(J)/(S2*N))
1160  PRINT "DATA ERROR IN PARAMETER "J" IS" SQR(R1(J)/(S2*N))
1170  NEXT J
1180  STOP
1190  FOR K=1 TO 3
1200  N(K)=3.152E12*X(K)
1210  A1(K)=1E-15*P(2)*N(K)+1/R
1220  NEXT K
1230  G=EXP(-A1(3)*X3)
1240  G1=-1*X3*N(3)*G
1250  U=G*EXP(-A1(2)*X2)
1260  U1=-1*(X2*N(2)+X3*N(3))*U
1270  H=U*EXP(-A1(1)*x1)
1280  H1=-1*(X1*N(1)+X2*N(2)+X3*N(3))*H
1290  F2(1)=1E-12*(N(1)/A1(1)*(U-H)+N(2)/A1(2)*(G-U)+N(3)/A1(3)*(1-G))
1300  S=N(1)/A1(1)*(U1-H1)-(N(1)/A1(1))↑ 2*(U-H)+N(2)/A1(2)*(G1-U1)
1310  F2(2)=1E-27*(S-N(3)/A1(3)*G1-(N(3)/A1(3))↑ 2*(1-G)-(N(2)/A1(2))↑ 2
1311  & *(G-U))
1320  F1=F2(1)*P(1)
1330  RETURN
1340  END
```

REFERENCES

Bauer, E., R. Kumler and M. H. Bortner, Internal energy balance and energy transfer in the lower thermosphere, Applied Optics, 10, 1861, (1971).

Bottcher, C. and C. V. Sukumar, Quenching of excited atoms by collisions with stable molecules, J. Phys. B., 10, 2853, (1977).

Christensen, A.B., M. H. Rees, G. J. Romick and G. G. Sivjee, OI(7774 A) and OI(8446 A) emissions in aurora, J. Geophys. Res., 83, 1421, (1978).

Cohen, R. B., Formation of NO^+ by the reaction of O^+ and vibrationally excited N_2 in crossed molecular beams, J. Chem. Phys., 57, 676, (1972).

Hughes, B. M. and T. O. Tiernan, Determination of the abundance of excited O^+ ions in beams produced by electron impact on O_2, CO_2, N_2O, NO_2 and H_2O, J. Chem. Phys., 55, 3419, (1971).

Johnsen, R. and M. A. Biondi, Measurements of the $O^+ + N_2$ and $O^+ + O_2$ reaction rates from 300 ^oK to 2 eV, J. Chem. Phys., 59, 3504, (1973).

Kosmider, R. G. and J. B. Hasted, Collision processes of drifting O^+ and N^+ ions, J. Phys. B., 8, 273, (1975).

Neynaber, R. H. and G. D. Magnuson, Low-energy study of $O^+ + N_2 \rightarrow NO^+ + N^*$, J. Chem. Phys., 58, 4586, (1973).

O'Malley, T. F., Simple model for the high energy reaction of O^+ ions with N_2^*, J. Chem. Phys., 52, 3269, (1970).

Ormrod, J. H. and W. L. Michel, Charge equilibrium fractions and charge-exchange cross sections for fast ions in nitrogen and argon, Can. J. Phys., 49, 606, (1971).

Potter, R. F., Cross sections for charge transfer collisions of low-energy ions in N_2 and O_2, J. Chem. Phys., 22, 974, (1954).

Sharp, R. D., R. G. Johnson and E. G. Shelley, Observation of an ionospheric acceleration mechanism producing energetic (keV) ions primarily normal to the geomagnetic field direction, J. Geophys. Res., 82, 3324, (1977).

Shelley, E. G., R. D. Sharp and R. G. Johnson, Satellite observation of an ionospheric acceleration mechanism, J. Geophys. Res. Lett., 3, 654, (1976).

Solove'v, E. S., R. N. Il'in, V. A. Oparin, I. T. Serenkov and N. V. Fedorenko, Capture and loss of electrons by fast nitrogen and oxygen atoms in air, N_2 and O_2, Soviet Phys.- Tech. Phys., 17, 267, (1972).

Stebbings, R. F., Ben R. Turner and A. C. H. Smith, Charge transfer in oxygen, nitrogen and nitric oxide, J. Chem. Phys. 38, 2277, (1963).

Turner, B. R., J. A. Rutherford and D. M. J. Compton, Abundance of excited ions in O^+ and O_2^+ ion beams, J. Chem. Phys., 48, 1602, (1968).

Weise, W. L., M. W. Smith and B. M. Glennon, Atomic Transition Probabilities, National Standard Reference Data Series, National Bureau of Standards 4, 79, (1966).